Polymer 53 (2012) 2306–2314

Contents lists available at SciVerse ScienceDirect

Polymer

journal homepage: www.elsevier.com/locate/polymer

Low-molecular weight aliphatic amides as nucleating agents for poly (L-lactic acid): Conformation variation induced crystallization enhancement

Qian Xing [a], Xiuqin Zhang [b], Xia Dong [a], Guoming Liu [a], Dujin Wang [a,*]

[a] Beijing National Laboratory for Molecular Sciences, CAS Key Laboratory of Engineering Plastics, Institute of Chemistry, Chinese Academy of Sciences, Beijing 100190, PR China
[b] Beijing Key Laboratory of Clothing Materials R & D and Assessment, Department of Materials Science & Engineering, Beijing Institute of Fashion Technology, Beijing 100029, PR China

ARTICLE INFO

Article history:
Received 11 November 2011
Received in revised form
4 March 2012
Accepted 18 March 2012
Available online 23 March 2012

Keywords:
Poly (L-lactic acid)
Aliphatic amide
Nucleating efficiency

ABSTRACT

Two kinds of low molecular weight aliphatic amides, *N*, *N*′-ethylenebis (12-hydroxystearamide) (EBH) and *N*, *N*′-ethylenebisstearamide (EBSA), have been selected in present study to mediate the crystallization behavior of poly (L-lactic acid) (PLLA). The results showed that the crystallization rate of PLLA was significantly improved with the addition of EBH and EBSA, and EBH presented a stronger nucleating efficiency. The correlation between the variation of chain conformation during the early stages of isothermal crystallization and the enhancement of crystallization rate for pure PLLA and its mixtures was investigated by time-resolved FTIR. The formation of interchain conformational-ordered structure and intrachain 10_3 helix structure for amide-doped PLLA preceded that for pure PLLA, suggesting a stimulatory nucleating effect of EBH and EBSA. In the case of PLLA/EBH, the interchain interactions of $-(COC + CH_3)$ and $-CH_3$ groups were faster than the $-(CH_3+CC)$ intrachain interactions, while the interchain interactions and the intrachain 10_3 helix formation were nearly synchronous for PLLA/EBSA. The hydrogen bond interaction between hydroxyl groups in EBH and the carbonyl groups in PLLA was proposed to be an important factor influencing the conformation variation during isothermal crystallization of PLLA.

1. Introduction

Poly (L-lactic acid) (PLLA) is one of the most important biocompatible and biodegradable polymers, the monomers of which are generally produced by fermentation of renewable natural resources like corn and sugar cane [1], etc. PLLA not only has been widely used in biomedical applications such as surgical sutures and controlled drug delivery systems [2–4], but also has substituted some conventional plastics to a certain extent [5–8], due to its good mechanical properties. However, the crystallization rate of PLLA is rather slow, which leads to a long processing period and poor heat resistance, limiting its extensive applications. Numerous studies have been carried out for improving the crystallization rate of polymers, such as blending with other polymers [9–13] and addition of inorganic additives [14–20], etc. Sakai et al. [9] showed that only a small amount of PCL can improve the crystallization rate of PLLA significantly. The PLLA chain mobility at the interface between PCL domains and PLLA matrix was activated locally by the presence of PCL, contributing to the strong enhancement of PLLA nucleation. Krikorian et al. [16] studied the effect of organically modified montmorillonite clay on the crystallization of PLLA, and found that the overall bulk crystallization rate was increased in the intercalated system relative to neat PLLA. In PLLA composites prepared through addition of functionalized multiwalled carbon nanotubes (F-MWNTs) [19], the F-MWNTs acted as a nucleating agent to enhance the crystallization of PLLA when below the percolation concentration, while as a hindrance retarding the crystallization above the percolation concentration.

It has been reported that some organic compounds can also be used to promote the crystallization rate of PLLA, e g, decamethylenedicarboxylic dibenzoylhydrazide and citrate esters [21,22]. Among these organic compounds, low molecular weight aliphatic amides, *N*, *N*′-ethylenebis (12-hydroxystearamide) (EBH) and *N*, *N*′-ethylenebisstearamide (EBSA) with environmental friendliness, are usually used as lubricant, release agent or dispersing agent to enhance processability of polymers, while some researchers [23,24] have found that EBH and EBSA are efficient nucleating agents for PLLA crystallization. Nam et al. [23] observed that EBH crystallized at the very early stage of PLLA crystallization and acted as a nucleating agent for PLLA crystallization. As a result, typical transcrystallites formed at the interface between PLLA and EBH, and the overall crystallization rate of PLLA was increased.

* Corresponding author. Tel./fax: +86 10 82618533.
E-mail address: djwang@iccas.ac.cn (D. Wang).

0032-3861/$ – see front matter © 2012 Elsevier Ltd. All rights reserved.
doi:10.1016/j.polymer.2012.03.034

Harris et al. [24] suggested that EBSA can also improve both the isothermal and nonisothermal crystallization rate of PLLA as well as the crystallinity. These reports seldom concern the interaction between PLLA and EBH or EBSA at the molecular level, which is believed to influence the intramolecular movements and intermolecular packing of polymer chains during crystallization process.

Therefore, in present study, EBH and EBSA were selected to mediate the crystallization behavior of PLLA, and the nucleating efficiency of the two low-molecular weight aliphatic amides has been compared, based on their interactions with PLLA. The main aim is to compare the effect of EBH and EBSA on the crystallization behavior of PLLA and further explore their nucleating mechanisms. The interactions between EBH/EBSA and PLLA were illustrated at the molecular level during crystallization induction period before primary nucleation [14,25,26]. Time-resolved FTIR was applied to understand the conformational changes and crystalline ordering of PLLA by following the intensity and shape changes of characteristic bands [27,28]. It has been found that EBH shows much stronger nucleation efficiency for PLLA than EBSA, which might be attributed to the hydrogen bond interaction between hydroxyl groups in EBH and the carbonyl groups in PLLA.

2. Experimental section

2.1. Materials

PLLA of commercial grade 2002D with 4.6 wt% of D-isomer units was purchased from NatureWorks. The number-average molecular weight and weight-average molecular weight are 1.5×10^5 g/mol and 2.0×10^5 g/mol, respectively. The melt flow index is 3–4 g/10 min (190 °C/2.16 kg). The nucleating agent EBH was kindly supplied by Beijing University of Chemical Technology ($T_c = 130$ °C, $T_m = 142$ °C, DSC, 10 °C/min). EBSA was supplied by J & K Scientific Ltd. ($T_c = 142$ °C, $T_m = 146$ °C, DSC, 10 °C/min). The chemical structures of PLLA, EBH and EBSA are illustrated in Scheme 1. The received materials were dried in a vacuum oven for 24 h at 70 °C, and then stored in a desiccator before use.

2.2. Sample preparation

PLLA/EBH mixture was prepared by the solution casting method. 1 g PLLA was first dissolved in 100 ml chloroform at 50 °C, followed by the addition of 0.01 g EBH into the solution and stirring for 3 h. PLLA/ESBA mixture was prepared with the same method. Sample films for FTIR measurement were prepared by casting the solution onto KBr windows. Films for other tests including DSC, SEM and POM were prepared by casting solutions on glass dishes. The as-prepared films were kept in a vacuum oven 50 °C for 3 days, and then cooled to room temperature.

2.3. Scanning Electron Microscopy (SEM)

A JSM-6700F JEOL scanning electron microscope operated at 5 kV was applied to examine the dispersion of EBH and EBSA in PLLA. A platinum layer was deposited on the surface of obtained films prior to SEM observation.

2.4. Transmission Electron Microscopy (TEM)

The spin-coating method was applied to prepare the specimens for transmission electron microscopic measurement. Samples for TEM observation were collected from water on 300 mesh carbon-coated copper grids. TEM imaging was performed on a Hitachi H-800 electron microscope operated at an accelerating voltage of 100 kV.

2.5. Differential Scanning Calorimetry (DSC)

The crystallization behavior of PLLA and its mixtures with EBH or EBSA were measured on a Perkin–Elmer DSC-7 analyzer. The temperature and heat flow were calibrated by using indium as the standard. The measurements were conducted under nitrogen atmosphere. The samples of about 5 mg were weighed and sealed in an aluminum pan, heated to 200 °C and held for 3 min to eliminate the thermal history. For the non-isothermal crystallization measurement, the samples were first cooled to 50 °C at 2 °C/min, and then heated to 200 °C at 10 °C/min. In the case of isothermal crystallization measurement, the samples were quenched to 125 °C at 40 °C/min and held until the samples crystallized completely.

2.6. Polarized Optical Microscopy (POM)

The nucleation and growth of PLLA spherulites during isothermal crystallization were observed with an Olympus BX51 polarized optical microscope equipped with a Canon 40D camera system. The temperature was controlled by a Linkam LTS 350 hot stage. The solution cast films with thickness of 30 μm were sandwiched by two glass slides, and then held at 200 °C for 3 min, followed by quenching to 125 °C for isothermal crystallization.

2.7. Fourier Transform Infrared Spectroscopy (FTIR)

FTIR spectra were measured by using a Bruker EQUINOX 55 spectrometer equipped with a DTGS detector in transmission mode. Time-resolved FTIR spectra were collected at a resolution of 2 cm^{-1} by averaging 16 scans with 1 min intervals for PLLA mixtures and 2 min intervals for pure PLLA. The background spectra used for reduction were collected at the same temperatures as the

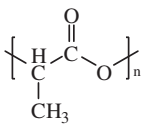

PLLA

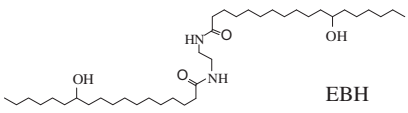

EBH

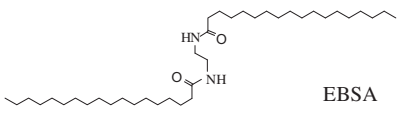

EBSA

Scheme 1. Chemical structures of PLLA, EBH and EBSA.

samples. The samples prepared by solution casting were set in an Instec Standalone Temperature Controller (STC 200), which was placed in the compartment of the spectrometer. Each sample was kept at 200 °C for 3 min to completely erase the thermal history and then cooled to 125 °C at 30 °C/min. When the temperature reached 125 °C, data collection started. The baseline of each spectrum was linearly corrected according to the same standard.

3. Results and discussion

3.1. Dispersion of EBSA and EBH in PLLA

In order to check the dispersion state of EBH and EBSA in PLLA matrix, the morphology of the as-received films was observed by SEM and TEM. It can be seen from Fig. 1 that EBH and EBSA are homogenously dispersed in PLLA matrix with the similar sizes in sub-microns, and the size distribution is narrow. The difference between the SEM and TEM images is attributed to the different preparation methods of the PLLA films. The films for SEM observation were solution casting prepared, while the TEM films were spin-coating results.

3.2. Nucleation effect of EBSA and EBH

The DSC thermograms for the non-isothermal crystallization of pure PLLA and its mixtures are shown in Fig. 2. The characteristic quantities are summarized in Table 1. In the cooling scan, there is almost no heat flow detected for pure PLLA, and only the crystallization peak of EBSA emerges at around 137.3 °C for PLLA/EBSA, indicating the slow crystallization rate of pure PLLA and PLLA in PLLA/EBSA mixture. For PLLA/EBH sample, however, there are two exothermic peaks at 121.8 and 109.6 °C assigned to the crystallization peaks of EBH and PLLA, suggesting that EBH effectively promotes the crystallization of PLLA during the cooling process.

In the following heating scan, pure PLLA and PLLA/EBSA samples exhibit large heat relaxation peaks accompanying the glass transition at around 63 °C, indicated by the arrows in Fig. 2b, which may be attributed to the rearrangement of amorphous molecular chains of PLLA. Cold crystallization peak emerges in PLLA/EBSA mixture at 126 °C, whereas no cold crystallization peak can be observed for pure PLLA. This indicates that EBSA can promote PLLA molecular chains to form ordered structures in the heating process, although it is not able to induce the crystallization of PLLA in the cooling scan. The melting enthalpies decrease as follows: PLLA/EBH, PLLA/EBSA, and pure PLLA. Thus, it is obvious that EBH and EBSA act as effective nucleating agents for PLLA crystallization, and EBH is much more efficient.

The isothermal crystallization traces of PLLA and its mixtures at 125 °C are shown in Fig. 3. The heat flow of pure PLLA changes very slow, and there is no visible crystallization peak in the experiment course. In contrast, PLLA/EBSA and PLLA/EBH show remarkable crystallization peaks. It's notable that the overall crystallization time of pure PLLA is much longer than that of PLLA mixtures, confirming that the addition of EBH and EBSA improves the crystallization rate of PLLA greatly. Compared with PLLA/EBSA, PLLA/EBH displays a sharper crystallization peak and a shorter crystallization time, meaning that EBH has stronger nucleating ability than EBSA, and the crystallization rate of PLLA in PLLA/EBH is faster than that of PLLA/EBSA.

The well-known Avrami equation [29] is described as Eq. (1):

$$1 - X_t = \exp(-Kt^n) \tag{1}$$

which is employed to analyze the isothermal crystallization kinetics of polymers, and its linear form is given as Eq. (2):

$$\ln[-\ln(1 - X_t)] = \ln K + n\ln t \tag{2}$$

where X_t is the relative degree of crystallinity at a given time t, which can be calculated from the integrated area of the DSC curve

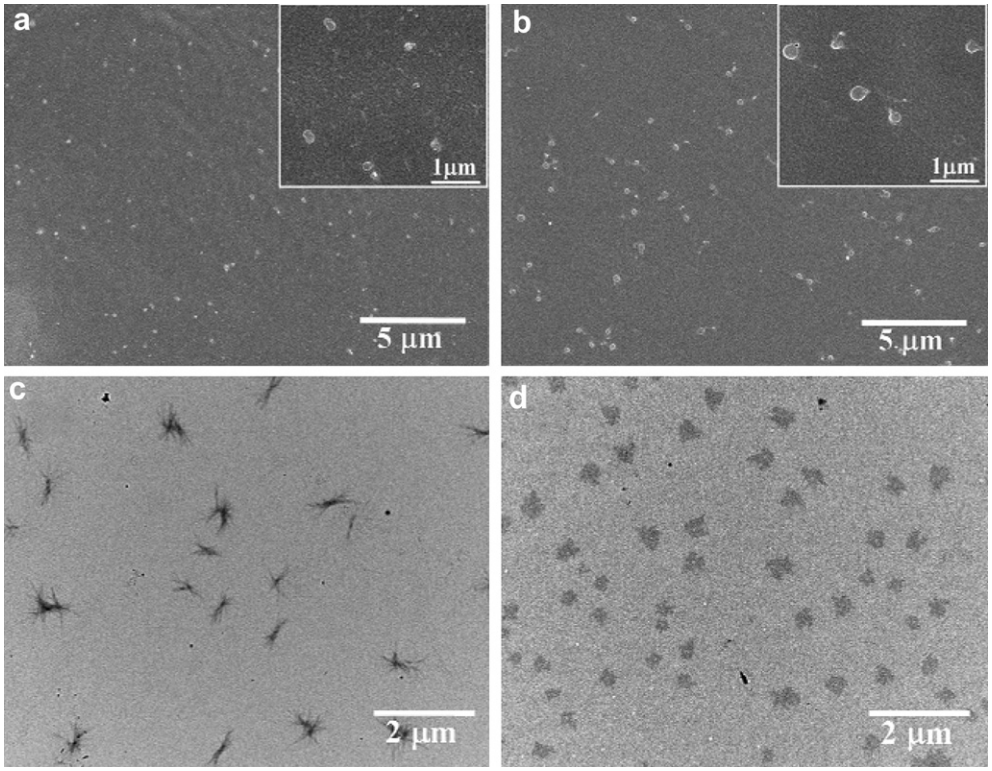

Fig. 1. SEM (a, b) and TEM (c, d) images showing the dispersion of EBH (a, c) and EBSA (b, d) in PLLA matrix. The insets are the high-magnification images.

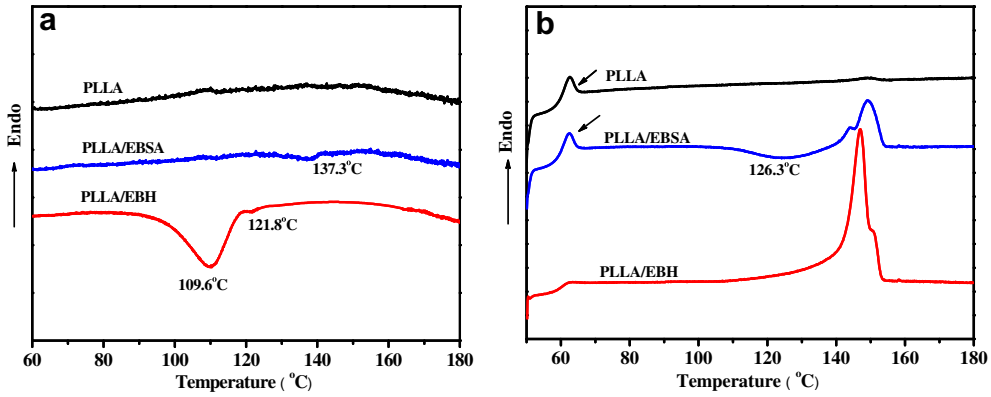

Fig. 2. DSC thermograms of pure PLLA and its mixtures: (a) cooling curves (2 °C/min), (b) heating curves (10 °C/min).

from $t = 0$ to $t = t$ divided by the integrated area of the whole heat flow curve. n is the Avrami index and K is the overall rate constant. The crystallization half-time $t_{0.5}$, defined as the time when X_t reaches 50%, can be determined from the X_t vs t plot. In Eq. (2), the unit of K is $\min^{-n}$, and n is not a constant. Thereafter, it is not reasonable to compare the total crystallization rate through K. The crystallization half-time $t_{0.5}$ calculated by Eq. (3) is applied to analyze the crystallization kinetics related to the bulk crystallization.

$$t_{0.5} = \left(\frac{\ln 2}{K}\right)^{1/n} \tag{3}$$

Fig. 4 shows the relative crystallinity as a function of crystallization time for PLLA mixtures. Because the heat flow in the isothermal crystallization of pure PLLA is hardly observed, its isothermal crystallization kinetics is not analyzed by Avrami equation. The curves of Avrami equation in Fig. 5 show a good linear fit for PLLA mixtures. The slope of the curves is the Avrami exponent n and the intercept is ln K.

Based on Figs. 4 and 5, the parameters of isothermal crystallization kinetics calculated by employing Avrami equation are listed in Table 2. The induction time is determined by the time required to detect a considerable increase in X_t relative to the initial stage. According to the nucleation and growth theory of polymer crystallization, the induction time is correlated to the nucleation characteristics of the system [14]. It can be seen that both $t_{0.5}$ and t_i of PLLA with the addition of EBH are shorter than those of PLLA in PLLA/EBSA, indicating that EBH reduces the induction period and the overall crystallization time more effectively.

The effect of nucleating agents on the crystalline morphology of PLLA was further observed with POM, and the results are shown in Fig. 6. There is nothing visible in the POM image of pure PLLA after isothermal crystallization at 125 °C for 10 min, indicating that the nucleation and crystal growth have not occurred within the observation time. However, a variety of tiny spherulites are formed in PLLA mixtures at the same experimental conditions. It can be seen that the nucleation density of PLLA/EBH is larger than that of PLLA/EBSA. Consequently, PLLA/EBH has a smaller spherulite size and shows a faster crystallization rate.

3.3. Time-resolved FTIR investigation on crystallization behavior

FTIR spectroscopy, which has been widely used for the characterization of polymers [30–34], is one of the most suitable means for the detection of conformational changes, crystal structure and the packing of the molecular chains. Furthermore, the crystallization kinetics can also be evaluated through tracing the variation of the characteristic bands during crystallization.

3.3.1. Band assignments

There are a variety of conformation sensitive and crystalline sensitive bands for PLLA. The spectral evolution during the isothermal crystallization process is shown in Fig. 7a–c. The difference spectra calculated by subtracting the initial spectrum from the rest of spectra in Fig. 7 a–c are depicted in Fig. 7d–e. In the difference spectra, the positive regions are crystalline-dependent, while the negative regions indicates the amorphous component. The specific assignments of the characteristic bands in the range 1500–830 cm^{-1} are summarized in Table 3 based on literature [25,35,36].

The band in the region from 1500 to 1000 cm^{-1} is highly sensitive to the crystallization process of PLLA [25,27]. As the crystallization progresses, the peak intensity changes and the peak position shifts. Compared with the original FTIR spectra, the difference spectra of pure PLLA and PLLA mixtures with EBH and EBSA show the band splitting phenomenon during isothermal crystallization. The band around 1454 cm^{-1}, attributed to the asymmetric deformation mode of CH_3, splits into two bands at 1458 and 1442 cm^{-1}, intensities of which increase with the crystallization time. The band at around 1200 cm^{-1} is ascribed to the asymmetric vibrations of C–O–C groups linked with asymmetric CH_3 rocking vibrations, and shifts to higher wavenumbers with the crystallization of PLLA. Furthermore, this band in the difference spectra also splits into two bands at 1210 and 1180 cm^{-1}. It is reported [37] that band splitting due to the dipole–dipole coupling occurs when the ordered structure of molecules forms in polymer systems. If the intermolecular forces between polymer chains are sufficient, the fundamental modes of a single polymer chain split into different spectral components. Thereafter, the band splitting at

Table 1
Crystallization and melting results for pure PLLA and its mixtures.

Samples	Crystallization		Cold crystallization		Melting	
	Temperature (°C)	Enthalpy (J/g)	Temperature (°C)	Enthalpy (J/g)	Temperature (°C)	Enthalpy (J/g)
PLLA	–	–	–	–	149.6	0.5
PLLA/EBSA	137.3	–	126.3	5.0	144.1/149.3	8.3
PLLA/EBH	121.8/109.6	22.9	–	–	146.9/151.3	30.7

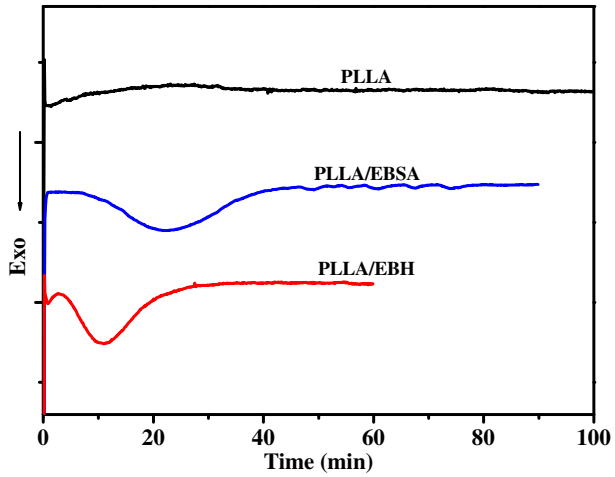

Fig. 3. DSC curves of pure PLLA and its mixtures isothermally crystallized at 125 °C.

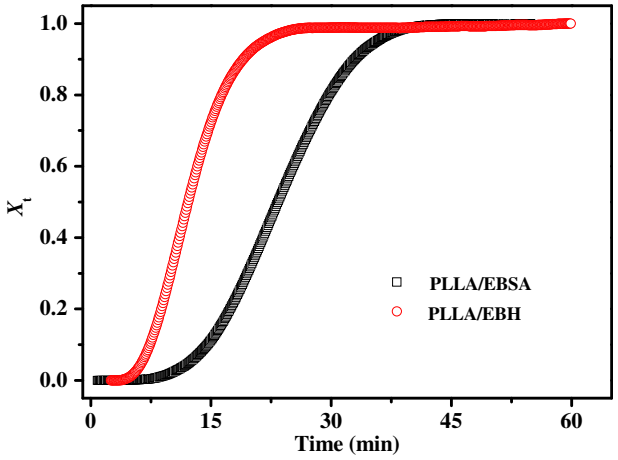

Fig. 4. The relative crystallinity (X_t) as a function of crystallization time for PLLA mixtures isothermally crystallized at 125 °C.

around 1458 and 1200 cm^{-1} may be caused by the dipole–dipole interaction due to the interchain packing in the crystal unit cell of PLLA and its mixtures. It is reasonable to correlate the changes of the band at around 1458 and 1210 cm^{-1} with interchain interaction. On the other hand, the band at 1267 cm^{-1}, ascribed to the

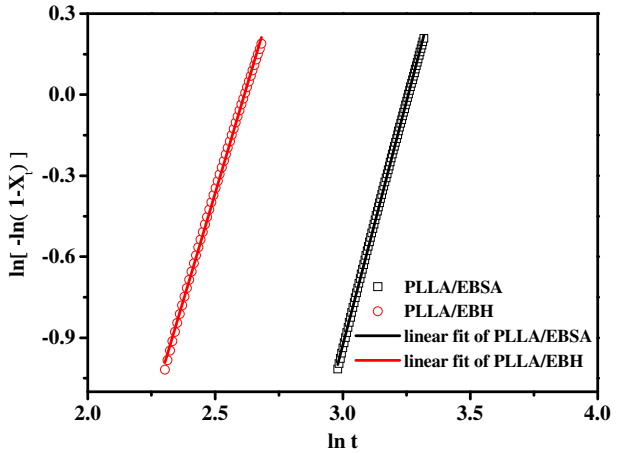

Fig. 5. The Avrami plot of PLLA mixtures isothermally crystallized at 125 °C.

Table 2
The Avrami parameters of PLLA mixtures.

Samples	Induction time t_i (min)	Crystallization half-time $t_{0.5}$ (min)	n	K (min^{-n})
PLLA/EBSA	5.8	23.9	3.6	7.66×10^{-6}
PLLA/EBH	3.3	12.0	3.2	2.46×10^{-4}

C–O–C asymmetric vibration linked with the CH deformation mode of the less energy-favorable *gg* conformers of PLLA, is sensitive to the amorphous phase of PLLA [28,38], and its intensity decreases with crystallization time.

The band ranging from 960 to 830 cm^{-1} is sensitive to the degree of crystallinity [25,28]. The bands at around 920 and 956 cm^{-1}, arising from the coupling of C–C backbone stretching

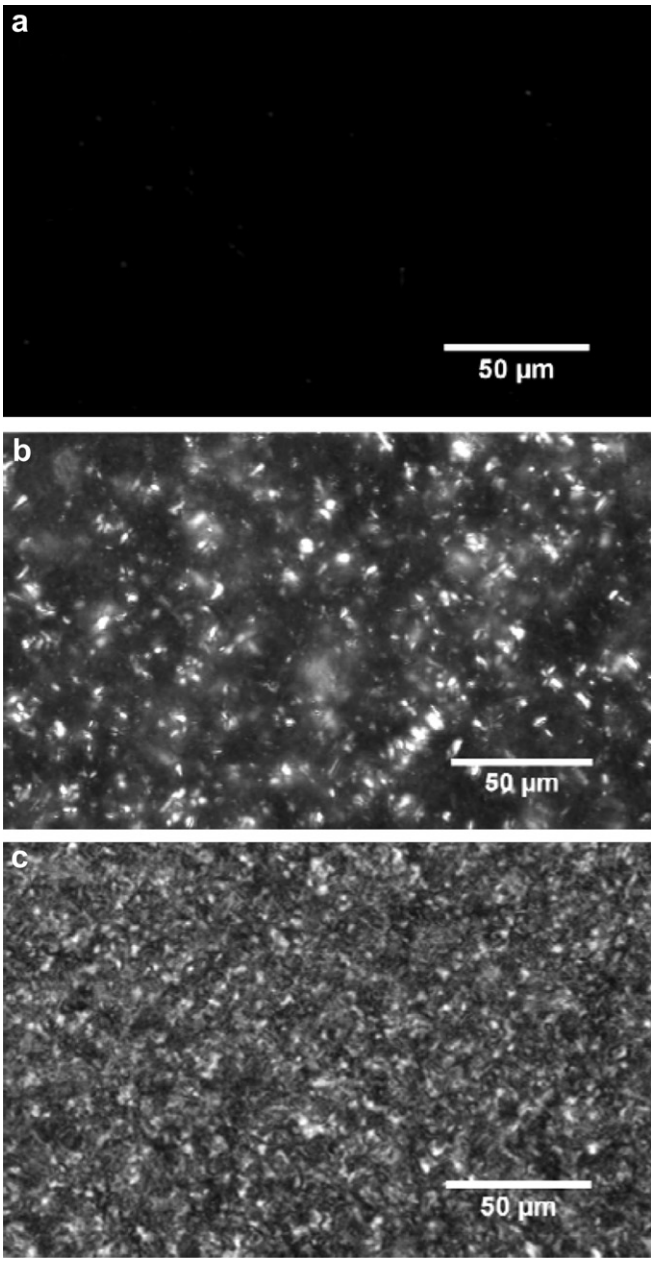

Fig. 6. POM images of (a) pure PLLA, (b) PLLA/EBSA and (c) PLLA/EBH isothermally crystallized at 125 °C for 10 min.

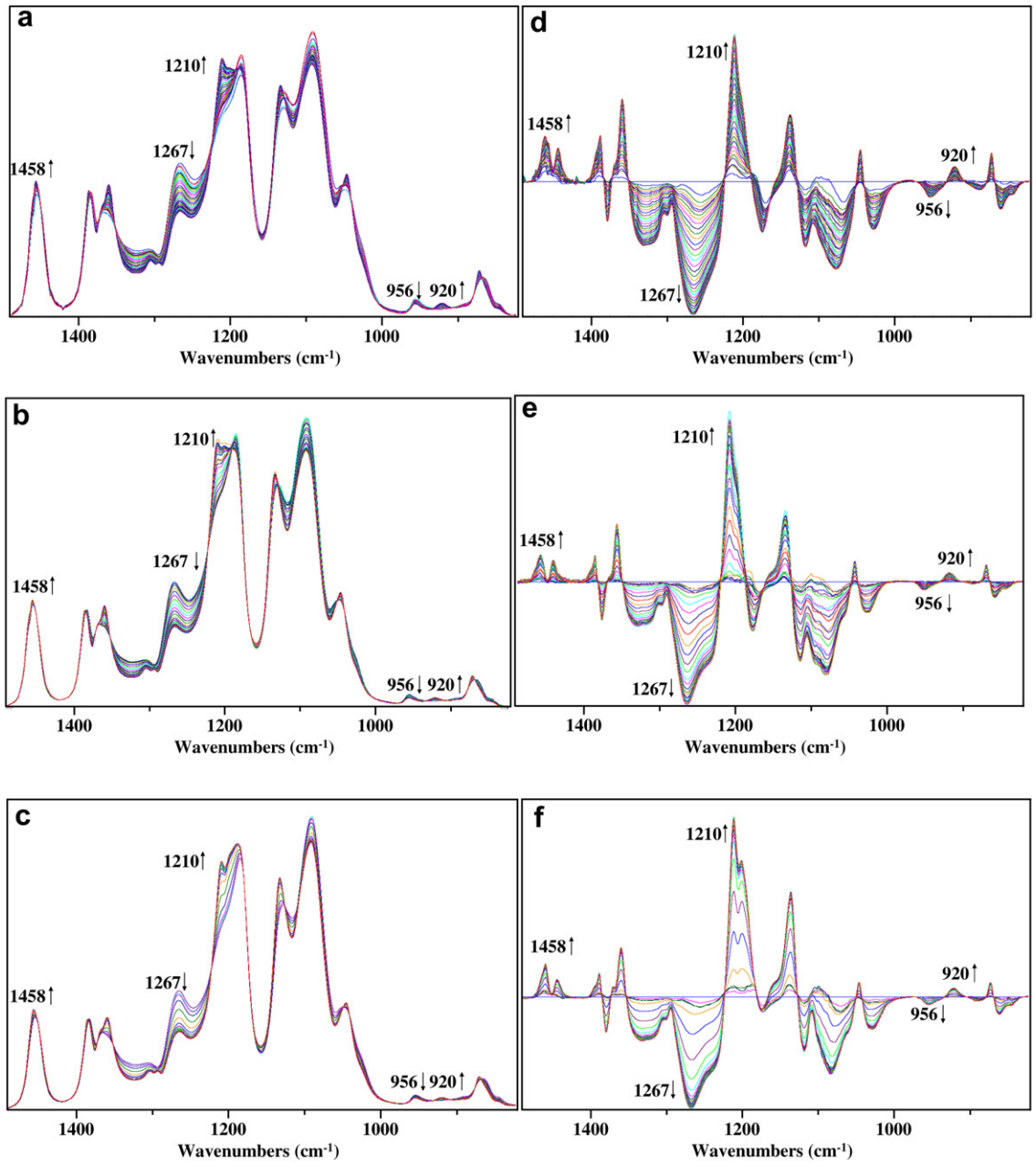

Fig. 7. Time-resolved FTIR spectra of PLLA (a), PLLA/EBSA (b), and PLLA/EBH (c) isothermally crystallized at 125 °C; and the corresponding difference spectra of PLLA (d), PLLA/EBSA (e), and PLLA/EBH (f). (The spectra of PLLA were stacked every 16 min, and the spectra of the mixtures were stacked every 2 min).

and the CH_3 rocking mode, are assigned to the crystalline phase of α-form in PLLA crystals and the amorphous phase, respectively. The α-form is the lowest energy conformation of single PLLA chain with a distorted 10_3 helix conformation [39]. In the initial stage of crystallization, the peak at around 920 cm^{-1} cannot be detected, suggesting the absence of crystals, while it emerges and the peak intensity increases monotonously as the crystallization progresses. In contrast, the peak intensity of band at 956 cm^{-1} decreases gradually. The band at around 865 cm^{-1}, corresponding to the stretching mode of C–COO, shifts to higher wavenumbers and becomes sharper, indicating a transition from disorder to ordered structure.

Table 3
Band assignments of PLLA in the 800–1500 cm^{-1} region.

Wavenumbers (cm^{-1})	Assignments	
1454	$\delta_{as}(CH_3)$	Conformation-sensitive,
1209–1186	$\upsilon_{as}(COC) + \gamma_{as}(CH_3)$	interchain interaction
1267	$\upsilon_{as}(COC) + \delta(CH)$	Conformation sensitive
956	$\gamma(CH_3) + \upsilon(CC)$	Amorphous-specific
920		Crystalline-specific, 10_3 helix formation sensitive, intrachain interaction
865	υ(C–COO)	Crystalline-specific

3.3.2. *Isothermal crystallization kinetics*

As mentioned above, the bands at 920 and 956 cm^{-1} are assigned to a 10_3 helix sensitive band and an amorphous band, respectively. They are well separated in the original IR spectra. Therefore, it is possible to determine the relative crystallinity (X_r) of pure PLLA and its mixtures by using the intensity ratio of the two bands (Eq. (4)).

$$X_r = A_{920}/A_{956} \quad (4)$$

The calculated relative crystallinity is shown in Fig. 8. The overall crystallization time t is obtained by the time when X_r reaches a plateau, and the induction time t_i is defined by the time when the considerable increase of X_r relative to the initial stage can be detected. As shown in Table 4, the values of t and t_i are the largest for pure PLLA, followed by PLLA/EBSA and PLLA/EBH. The addition of EBH and EBSA reduces the induction time and the overall crystallization time of PLLA remarkably, and EBH acts as a much more efficient nucleating agent to accelerate the crystallization of PLLA. Therefore, the FTIR results are in good agreement with the DSC data.

The difference in crystallization behaviors of pure PLLA and its mixtures may pertain to different conformational transformation during isothermal crystallization. With time-resolved FTIR spectroscopy, the origin and mechanism of the nucleating effects of EBH and EBSA on PLLA crystallization can be elucidated. The normalized peak intensity $X_{IR,t}$ of pure PLLA and its mixtures can be calculated by Eq. (5), where I_t is the peak intensity at the crystallization time t, and I_0 and I_∞ are the initial and final peak intensities during isothermal crystallization, respectively.

$$X_{IR,t} = \frac{I_t - I_0}{I_\infty - I_0} \times 100\% \quad (5)$$

The normalized intensities at 1210, 1458, and 920 cm^{-1} are plotted as a function of crystallization time (Fig. 9), so as to qualitatively compare the variations of 10_3 helix sensitive bands and the skeletal vibrations over the course of crystallization. The bands at 1210 and 1458 cm^{-1} are conformation-sensitive, while 920 cm^{-1} is a pure crystalline band and sensitive to 10_3 helix formation in PLLA crystalline phase. As is reported [25,40], the former conformation-sensitive bands are representative of the interchain interactions, while the latter crystalline band is correlated to the intrachain interactions. Both t_i and $t_{0.5}$ of PLLA mixtures are shorter than those of pure PLLA for each band, indicating that the formation of the ordered skeletal conformation and 10_3 helix structure occurs in the earlier stage compared with that in pure PLLA. It can be seen that EBH and EBSA promotes the occurrence of both the interchain interactions and intrachain interactions, and thus the crystallization rate of PLLA is enhanced. The t_i and $t_{0.5}$ associated with PLLA/EBH is the shortest, suggesting the faster nucleation rate and bulk crystallization kinetics than pure PLLA and PLLA/EBSA.

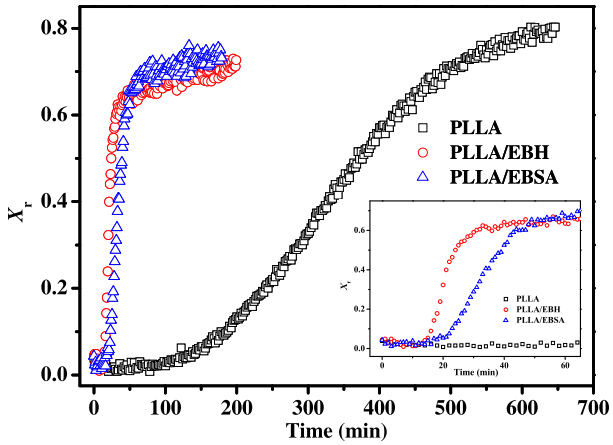

Fig. 8. The relative crystallinity of pure PLLA and its mixtures as a function of crystallization time at 125 °C.

Table 4
Crystallization kinetics parameters obtained from time-resolved FTIR.

Samples	Induction time t_i (min)	Overall crystallization time t (min)
PLLA	100	640
PLLA/EBSA	16	84
PLLA/EBH	11	50

To compare the variation of skeletal conformational order and helix formation, normalized peak intensities at 920, 1210 and 1458 cm^{-1} are presented as a function of crystallization time (Fig. 10). The order of intensity changes in the earlier stages is as follows:

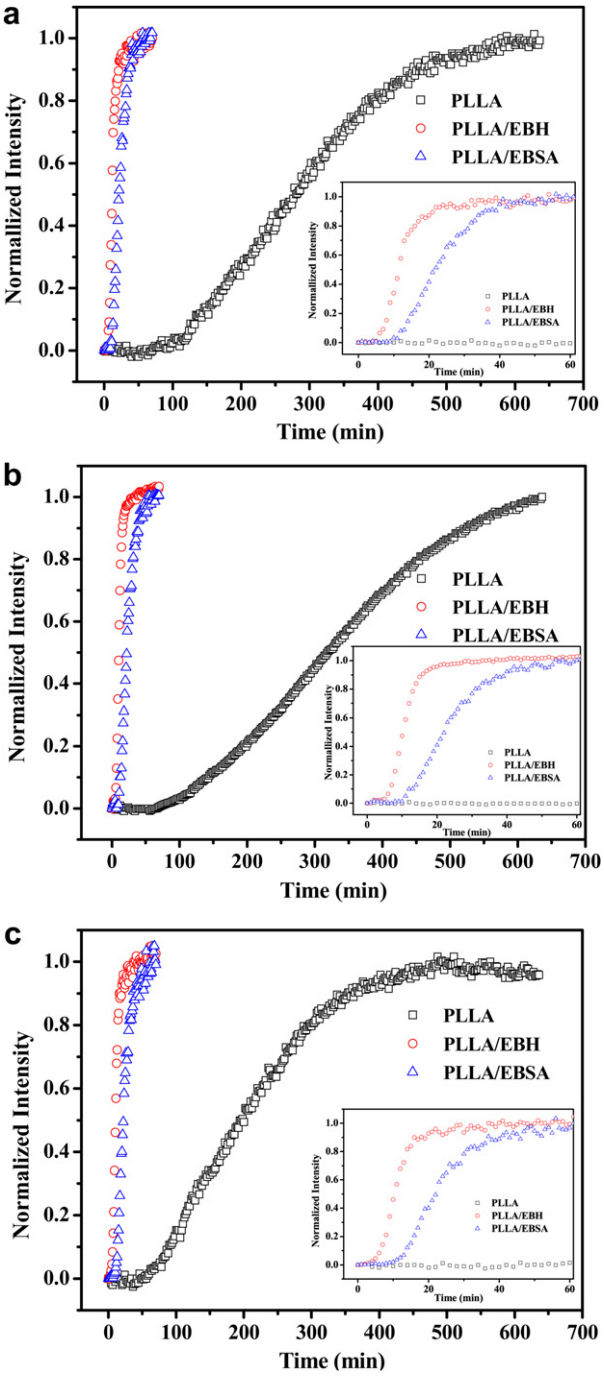

Fig. 9. Normalized peak intensities at 920 (a), 1210 (b) and 1458 cm^{-1} (c) as a function of crystallization time for pure PLLA, PLLA/EBSA, and PLLA/EBH.

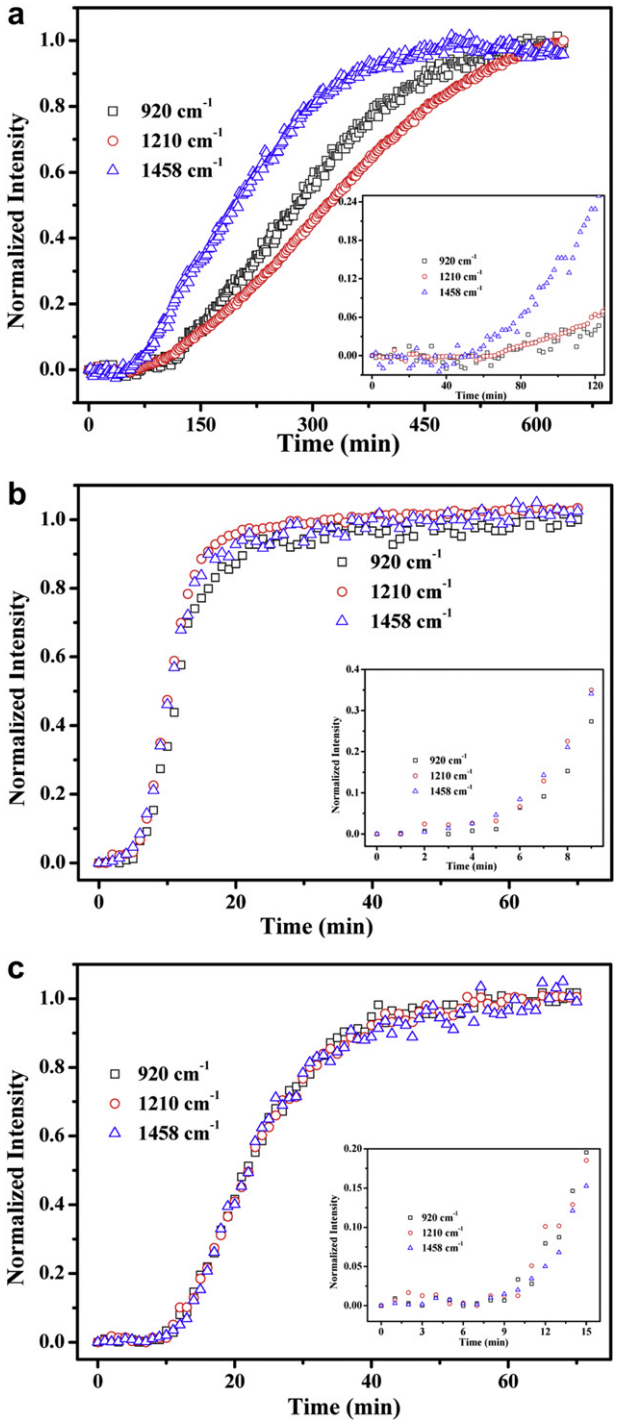

Fig. 10. Normalized peak intensities at 920, 1210, and 1458 cm^{-1} as a function of crystallization time for pure PLLA and its mixtures. PLLA (a), PLLA/EBH (b), and PLLA/EBSA (c).

PLLA: 1458 cm^{-1} > 1210 cm^{-1} ~ 920 cm^{-1}
PLLA/EBH: 1458 cm^{-1} ~ 1210 cm^{-1} > 920 cm^{-1}
PLLA/EBSA: 1458 cm^{-1} ~ 1210 cm^{-1} ~ 920 cm^{-1}

During the crystallization induction period of pure PLLA (Fig. 10a), the change of band at 1458 cm^{-1} is detected considerably earlier than that of bands at 1210 and 920 cm^{-1}. This suggests that the δ_{as} (CH_3) interchain interactions precede that the υ_{as} (COC)+γ_{as} (CH_3) interchain interactions and 10_3 helix formation. In Fig. 10b, for PLLA/EBH, the intensity changes of bands at 1458 and 1210 cm^{-1} start at a similar stage and are prior to the change of band at 920 cm^{-1}. This means that the interchain interactions corresponding to δ_{as} (CH_3) and υ_{as} (COC) + γ_{as} (CH_3) take place simultaneously, and they dominate the creation of stable nuclei which act as precursors for the formation of 10_3 helix structure. Otherwise, for PLLA/EBSA (Fig.10c), it's difficult to distinguish the difference in intensity changes of bands at 1458, 1210 and 920 cm^{-1}, implying that the interchain interactions and 10_3 helix formation occur synchronously.

The differences in kinetics of skeletal conformational ordering and helix formation signify the different crystallization mechanisms for pure PLLA and its mixtures. The conformational evolution of pure PLLA with the beginning of $-CH_3$ interchain interactions is prior to the intrachain 10_3 helix formation, which is requisite for the stable nucleus. This result is in well accordance with the extensive research in literature where for pure PLLA long-range order has been observed earlier than the formation of crystalline short-range order in the crystallization induction time [26,37,41]. However, it should take a long time for PLLA molecular chains to form an ordered conformation, since there is no extra drive for the interchain interactions. In the case of PLLA/EBH, the hydroxyl groups in EBH might interact with the carbonyl groups in PLLA main chains through hydrogen bonding, which acts as a template to adsorb the molecular chains. As reported in previous literature [42], in nylon-6/clay nanocomposites systems, one molecular layer is nucleated on the clay surface through hydrogen bonding during crystallization, thus preparing the surface for interaction with the subsequent molecules. This gives rise to a pseudo-hexagonally packed lamellar structure on both sides of the clay and promotes the crystallization of nylon-6. In the present case, the PLLA backbones may contact with the preadsorbed ones, promoting the formation of conformational ordered structure. Meanwhile, the $-CH_3$ groups among different PLLA chains are in close contact, and they can easily interact with each other. Correspondingly, the band at 1210 cm^{-1} in relation to υ_{as} (COC) + γ_{as} (CH_3) and the band at 1458 cm^{-1} to δ_{as} (CH_3) start to increase. The interchain interactions dominate the creation of stable nuclei and induce the following formation of 10_3 helix structure. In PLLA/EBSA, EBSA serves as a heterogeneous nucleus to induce skeletal conformational ordered structure and 10_3 helix formation. The interchain interactions are detected synchronously with the 10_3 helix formation, and thus it is not able to serve as efficient nucleating precursors with respect to EBH. Therefore, the nucleating effect of EBSA is weaker, and the overall crystallization rate of PLLA/EBSA is slower than that of PLLA/EBH.

Based on above discussion, it can be concluded that the interaction between EBH (or EBSA) and PLLA plays a critical role in the crystallization of PLLA, which generates different chain packing and skeletal conformation changes. As a consequence, the nucleation efficiency of the two low molecular weight amides differs from each other.

4. Conclusions

The effect of EBH and EBSA on the crystallization behavior of PLLA has been investigated in this work. The addition of EBSA and EBH can improve the crystallization of PLLA during non-isothermal crystallization and isothermal crystallization, and EBH shows much stronger nucleating ability than that of EBSA. Time-resolved FTIR spectroscopic investigation indicates that the formation of both skeletal conformational-ordered structure and 10_3 helix structure of amide-doped PLLA precedes that of pure PLLA. For pure PLLA, during isothermal crystallization, the $-CH_3$ interchain interactions at 1458 cm^{-1} occurs before the -(COC + CH_3) interchain interactions at 1210 cm^{-1} and the intrachain 10_3 helix formation at

920 cm^{-1}. In the case of PLLA/EBH, the interchain interactions are faster than the intrachain interactions. The interchain interactions dominate the creation of stable nuclei which act as precursors inducing the subsequent formation of 10_3 helix structure. However, for PLLA/EBSA mixture, the skeletal conformational ordering and 10_3 helix formation are nearly synchronous. It is suggested that the hydrogen bond interaction between hydroxyl groups in EBH and the carbonyl groups in PLLA, may be responsible for the stronger effect of EBH on the nucleating ability and crystallization kinetics of PLLA, with respect to EBSA.

Acknowledgments

We would like to thank the financial support from the National Funds for Distinguished Young Scientists (50925313) and the National Natural Science Foundation of China (11179031and 50873112).

References

[1] Lim LT, Auras R, Rubino M. Progress in Polymer Science 2008;33(8):820–52.
[2] Fambri L, Pegoretti A, Fenner R, Incardona SD, Migliaresi C. Polymer 1997; 38(1):79–85.
[3] Ma Z, Gao C, Gong Y, Shen J. Biomaterials 2005;26(11):1253–9.
[4] Kim HD, Bae EH, Kwon IC, Pal RR, Nam JD, Lee DS. Biomaterials 2004;25(12): 2319–29.
[5] Gupta AP, Kumar V. European Polymer Journal 2007;43(10):4053–74.
[6] Garlotta D. Journal of Polymers and the Environment 2001;9(2):63–84.
[7] Aou K, Kang SH, Hsu SL. Macromolecules 2005;38(18):7730–5.
[8] Zhang W, Chen L, Zhang Y. Polymer 2009;50(5):1311–5.
[9] Sakai F, Nishikawa K, Inoue Y, Yazawa K. Macromolecules 2009;42(21): 8335–42.
[10] Tsuji H, Tashiro K, Bouapao L, Narita J. Macromolecular Materials and Engineering 2008;293(12):947–51.
[11] Stoclet G, Seguela R, Lefebvre JM. Polymer 2011;52(6):1417–25.
[12] Anderson KS, Hillmyer MA. Polymer 2006;47(6):2030–5.
[13] Lopez-Rodriguez N, Lopez-Arraiza A, Meaurio E, Sarasua JR. Polymer Engineering and Science 2006;46(9):1299–308.
[14] Hu X, An HN, Li ZM, Geng Y, Li LB, Yang CL. Macromolecules 2009;42(8): 3215–8.
[15] Li YL, Wang Y, Liu L, Han L, Xiang FM, Zhou ZW. Journal of Polymer Science Part B-Polymer Physics 2009;47(3):326–39.
[16] Krikorian V, Pochan DJ. Macromolecules 2004;37(17):6480–91.
[17] Krikorian V, Pochan DJ. Chemistry of Materials 2003;15(22):4317–24.
[18] Pan PJ, Zhu B, Dong T, Inoue Y. Journal of Polymer Science Part B-Polymer Physics 2008;46(20):2222–33.
[19] Xu Z, Niu Y, Yang L, Xie W, Li H, Gan Z, et al. Polymer 2010;51(3):730–7.
[20] Lonkar SP, Morlat-Therias S, Caperaa N, Leroux F, Gardette JL, Singh RP. Polymer 2009;50(6):1505–15.
[21] Kawamoto N, Sakai A, Horikoshi T, Urushihara T, Tobita E. Journal of Applied Polymer Science 2007;103(1):198–203.
[22] Labrecque LV, Kumar RA, Dave V, Gross RA, McCarthy SP. Journal of Applied Polymer Science 1997;66(8):1507–13.
[23] Nam JY, Okamoto M, Okamoto H, Nakano M, Usuki A, Matsuda M. Polymer 2006;47(4):1340–7.
[24] Harris AM, Lee EC. Journal of Applied Polymer Science 2008;107(4):2246–55.
[25] Krikorian V, Pochan DJ. Macromolecules 2005;38(15):6520–7.
[26] Matsuba G, Kaji K, Nishida K, Kanaya T, Imai M. Macromolecules 1999;32(26): 8932–7.
[27] Zhang JM, Tsuji H, Noda I, Ozaki Y. Macromolecules 2004;37(17):6433–9.
[28] Pan P, Liang Z, Zhu B, Dong T, Inoue Y. Macromolecules 2008;41(21):8011–9.
[29] Avrami M. Journal of Chemical Physics 1939;7(12):1103–12.
[30] Kim HJ, Kim SB, Kim JK, Jung YM, Ryu DY, Lavery KA, et al. Macromolecules 2006;39:408–12.
[31] Snyder RW, Thomson B, Bartges B, Czerniawski D, Painter PC. Macromolecules 1989;22(11):4166–72.
[32] High MS, Painter PC, Coleman MM. Macromolecules 1992;25(2):797–801.
[33] Coleman MM, Skrovanek DJ, Hu JB, Painter PC. Macromolecules 1988;21(1): 59–65.
[34] Kobayashi M, Nakaoki T, Ishihara N. Macromolecules 1990;23(1):78–83.
[35] Kister G, Cassanas G, Vert M. Polymer 1998;39(2):267–73.
[36] Kang S, Hsu SL, Stidham HD, Smith PB, Leugers MA, Yang X. Macromolecules 2001;34(13):4542–8.
[37] Zhang JM, Tsuji H, Noda I, Ozaki Y. Journal of Physical Chemistry B 2004; 108(31):11514–20.
[38] Zhang JM, Li CW, Duan YX, Domb AJ, Ozaki Y. Vibrational Spectroscopy 2010; 53(2):307–10.
[39] Lin TT, Liu XY, He C. Polymer 2010;51(12):2779–85.
[40] Xu JZ, Chen T, Yang CL, Li ZM, Mao YM, Zeng BQ, et al. Macromolecules 2010; 43(11):5000–8.
[41] Jiang Y, Gu Q, Li L, Shen DY, Jin XG, Chan CM. Polymer 2003;44(12):3509–13.
[42] Maiti P, Okamoto M. Macromolecular Materials and Engineering 2003;288(5): 440–5.